Electronic Supplementary Material (ESI) for Chemical Science.

Bidirectional photoswitchability in an iron(III) spin crossover complex: Symmetry-breaking and solvent effects

Raúl Díaz-Torres,[a] Guillaume Chastanet,[b] Eric Collet,[c] Elzbieta Trzop,[c]

Phimphaka Harding*[d] and David J. Harding*[d]

[a] Thammasat University Research Unit in Multifunctional Crystalline Materials and Applications (TU-MCMA), Faculty of Science and Technology, Thammasat University, Pathum Thani 12121, Thailand
Previous address: Functional Materials and Nanotechnology Centre of Excellence, Walailak University, Thasala, Nakhon Si Thammarat, 80160, Thailand

[b] Université de Bordeaux, ICMCB, 87 avenue du Dr A. Schweitzer, Pessac, F-33608, France

[c] Univ Rennes, CNRS, IPR (Institut de Physique de Rennes) - UMR 6251, F-35000 Rennes, France

[d] School of Chemistry, Institute of Science, Suranaree University of Technology, Nakhon Ratchasima, 30000, Thailand
Previous address: Functional Materials and Nanotechnology Centre of Excellence, Walailak University, Thasala, Nakhon Si Thammarat, 80160, Thailand

E-mail: david@g.sut.ac.th or phimphaka@g.sut.ac.th

Contents Page No.

EXPERIMENTAL DETAILS

Materials. All reactions were carried out in aerobic conditions using commercial grade solvents for the synthesis of all compounds. All chemicals were purchased from TCI Chemicals or Sigma-Aldrich and used as received. Hqsal-I ligand was prepared as previously reported.[1]

Synthesis of $[Fe(qsal\text{-}I)_2]NO_3\cdot 2MeOH$ 1: Hqsal-I (74.8 mg, 0.2 mmol) was dissolved in DCM (3 mL) giving an orange solution. NEt_3 (28 μL, 0.2 mmol) was added and the solution was stirred for 5 min resulting in a change to dark orange. Next, blank MeOH (5 mL) was layered on the top of the Hqsal-I solution. In a separate flask, $Fe(NO_3)_3\cdot 9H_2O$ (40.4 mg, 0.1 mmol) was dissolved in MeOH (5 mL), filtered and then layered on the top of the previous solution and left for 4 days. The black crystals were formed (58 mg, 66 %). Anal. Calcd. for $FeC_{32}H_{22}O_6N_5I_2$ (882.21 $g\cdot mol^{-1}$): C 43.56 %, H 2.51 %, N 7.94 %. Found: C 43.99 %, H 2.61 %, N 7.74 %. ESI^+ (m/z): 802.0 $[Fe(qsal\text{-}I)_2]^+$. IR Data (KBr, cm^{-1}): 3045 ($\nu_{C\text{-}H}$), 1598 ($\nu_{C=N}$), 1384 ($\nu_{N\text{-}O}$).
Note: While elemental analysis is for the desolvated complex due to solvent loss during transport for EA, all structural, magnetic, powder diffraction and TGA data were conducted on fresh samples which clearly contain MeOH.

Synthesis of $[Fe(qsal\text{-}I)_2]NO_3\cdot 2EtOH$ 2: The same procedure as above was followed but substituting MeOH for EtOH (61 mg, 69 %). Anal. Calcd. for $FeC_{32}H_{20}I_2N_5O_5\cdot 2EtOH$ (940.28 $g\cdot mol^{-1}$): C 45.98 %, H 3.43 %, N 7.45 %. Found: C 45.82 %, H 3.34 %, N 7.52 ESI^+ (m/z): 801.9 $[Fe(qsal\text{-}I)_2]^+$ IR Data (KBr, cm^{-1}): 3039 ($\nu_{C\text{-}H}$), 1598 ($\nu_{C=N}$), 1382 ($\nu_{N\text{-}O}$).

X-ray Crystallography

The diffraction data of **1**-**2** were collected on a Rigaku SuperNova diffractometer with a HyPix 3000 detector using Cu Kα radiation (λ = 1.54184 Å). Photocrystallographic single-crystal X-ray studies of **1** were performed at 10 K on an Oxford Diffraction Xcalibur3 diffractometer, using MoKα radiation (λ = 0.71073 Å) and fitted with the Helijet Oxford Diffraction Cryostat. Irradiation of **1** took place at the thermally reached intermediate [HS-LS] state. Data collections were taken both before and after irradiation with 660 nm (at *ca.* 2 mW power) cw-laser reaching full conversion to LS state, and then, from LS state with 980 nm (at *ca*. 6 mW power) cw-laser reaching photoinduced HS state.

In all cases, data reduction, scaling, and absorption corrections were performed using CrysAlisPro.[2] The structures were solved, and the space group $P\bar{1}$ was determined by intrinsic phasing using ShelXT[3] and refined by full matrix least-squares minimization on F^2 using SHELXL.[4] All non-hydrogen atoms were refined anisotropically. Hydrogen atoms were

included in calculated positions and refined with isotropic thermal parameters, which were 1.2× the equivalent isotropic thermal parameters of their parent carbon atoms. When necessary SHELXL constrains and/or restrains have been applied. All pictures were generated with OLEX2.[5] Crystallographic data for the structures have been deposited with the Cambridge Crystallographic Data Centre (CCDC) under: 2220036-2220047. Powder X-ray diffraction data were measured on a Rigaku SuperNova diffractometer with a HyPix 3000 detector using Cu-Kα radiation (λ = 1.54184 Å). The samples were grounded and then suspended in Fomblim Y oil, and the data were collected between 2θ = 5−80°.

Physical measurements

Infrared spectra (4000−400 cm^{-1}) were recorded as KBr pellets on a PerkinElmer Spectrum One infrared spectrophotometer. Elemental analyses were carried out by using a Eurovector EA3000 analyzer. ESI-MS were carried out on a Bruker AmaZon X LCMS Mass Spectrometer. Magnetic measurements were performed using a MPMS 7XL SQUID Magnetometer from Quantum design, operating at 20 kOe of applied magnetic field at the same temperature scan rate of 0.5 K/min. The thermal spin crossover behaviours were recorded on sample wrapped in polypropylene bag which diamagnetic contribution was removed. The photoswitching was recorded directly in the SQUID magnetometer through an optical fibre placed close to the sample (6 cm). Irradiation was applied on a thin layer of compound and the thermal behavior after irradiation was recorded according to the T(LIESST) protocol.[6–8] The irradiations were provided by a home-made set of laser diodes.

Table S1 Spin state assignation, intermolecular interactions, interplanar and interchain distances of **1** and **2** at different temperatures. The compound $[Fe(qsal\text{-}Br)_2]NO_3 \cdot 2MeOH$ has also added for comparison.[9]

	$[Fe(qsal\text{-}I)_2]NO_3 \cdot 2MeOH$			**$[Fe(qsal\text{-}I)_2]NO_3 \cdot 2EtOH$**		**$[Fe(qsal\text{-}Br)_2]NO_3 \cdot 2MeOH$**		
Temperature	300 K	150 K		300 K	150 K	280 K	175 K	
Iron Centres	1	2		1	1	1	2	
	Fe1	Fe1	Fe2	Fe1	Fe1	Fe1	Fe1	Fe2
Spin state	HS	HS	LS	HS	LS	HS	HS	LS
π-π (Type A)	3.476	3.374	3.437	3.427	3.325	3.462	3.437	3.374
π-π (Type B)	3.337	3.287	3.319	3.306	3.254	3.339	3.327	3.286
(P4AE)CH···C_{cn}	2.753	2.663	2.748	2.902	2.911	2.679	2.611	2.649
(P4AE) π-π	3.686	3.603		3.906	3.876	3.396	3.379	
O···I (ROH)	3.094	3.068	2.975	3.185	3.052	3.163	3.227	2.990
O···I (NO_3)	3.508	3.498	3.624	3.378	3.384	3.609	3.610	3.730
d_{plane}	12.48	12.47	12.28	12.33	12.01	12.32	12.30	12.07
d_{chain}	12.01	12.23	11.72	12.29	12.31	12.02	12.27	11.77

Table S2 Selected Fe-N/O bond length (Å), volume cell (Å^3) and octahedral distortion parameters at various temperatures for all compounds. The Fe1 and Fe2 sites are equivalent at 300, 240 and 10 K after irradiation at 660 nm or 980 nm.

	$[Fe(qsal\text{-}I)_2]NO_3 \cdot 2MeOH$									
	1st cooling				**1st warming**	**2nd cooling**		**Dark**	**Irradiated (660 nm)**	**Irradiated (980 nm)**
	300 K	**240 K**	**150 K**	**100 K**	**300 K**	**240 K**	**150 K**	**10 K**	**10 K**	**10 K**
Fe1-O1ph	1.912(4)	1.908(3)	1.878(3)	1.876(4)	1.908(5)	1.906(5)	1.882(2)	1.883(2)	1.885(3)	1.914(2)
Fe1-O2ph	1.913(5)	1.913(3)	1.877(3)	1.883(4)	1.908(5)	1.914(5)	1.882(2)	1.884(2)	1.882(4)	1.909(3)
Fe1-Oph$_{av}$	1.913	1.911	1.877	1.879	1.908	1.910	1.882	1.884	1.883	1.911
Fe1-N1quin	2.160(5)	2.145(4)	1.979(6)	1.987(5)	2.140(5)	2.160(5)	1.983(3)	1.947(3)	1.969(4)	2.103(3)
Fe1-N2im	2.111(5)	2.099(3)	1.950(6)	1.947(4)	2.108(4)	2.109(5)	1.952(3)	1.987(2)	1.998(3)	2.136(3)
Fe1-N3quin	2.146(5)	2.132(4)	1.983(3)	1.982(5)	2.157(5)	2.135(6)	1.991(3)	1.947(3)	1.969(4)	2.107(3)
Fe1-N4im	2.113(5)	2.105(3)	1.952(3)	1.944(4)	2.118(4)	2.113(5)	1.952(3)	1.978(3)	2.008(4)	2.149(3)
Fe1-N$_{av}$	2.132	2.120	1.966	1.965	2.131	2.129	1.9695	1.964	1.986	2.123
Fe2-O3ph	-	-	1.915	1.915(4)	-	-	1.912(3)	1.914(2)	-	-
Fe2-O4ph	-	-	1.907	1.913(4)	-	-	1.913(2)	1.913(2)	-	-
Fe2-Oph$_{av}$	-	-	1.911	1.914			1.913	1.914	-	-
Fe2-N5quin	-	-	2.144	2.158(5)	-	-	2.143(3)	2.099(3)	-	-
Fe2-N6im	-	-	2.115	2.101(5)	-	-	2.110(3)	2.150(2)	-	-
Fe2-N7quin	-	-	2.161	2.138(5)	-	-	2.160(3)	2.100(3)	-	-
Fe2-N8im	-	-	2.117	2.106(4)	-	-	2.109(3)	2.131(3)	-	-
Fe2-N$_{av}$	-	-	2.134	2.125			2.131	2.120	-	-
V / Å^3	1699	1682	3316	3292	1702	1673	3316	3267	1631	1637
Σ-Fe1, Fe2	65	60	44, 65	43, 63	65	65	43, 64	44, 61	40	61
Θ-Fe1, Fe2	235	222	114, 247	110, 237	236	239	113, 242	114, 235	118	229

	$[Fe(qsal\text{-}I)_2]NO_3 \cdot 2EtOH$	
	1st cooling	
	300 K	**150 K**
Fe1-O1ph	1.904(3)	1.877(2)
Fe1-O2ph	1.898(4)	1.875(2)
$Fe1\text{-}Oph_{av}$	1.901	1.876
Fe1-N1quin	2.113(4)	1.984(3)
Fe1-N2im	2.083(4)	1.951(3)
Fe1-N3quin	2.128(3)	1.983(3)
Fe1-N4im	2.083(4)	1.944(3)
$Fe1\text{-}N_{av}$	2.102	1.965
V / Å³	1785	1732
Σ-Fe1, Fe2	60	45
Θ-Fe1, Fe2	204	117

Table S3 List of Fe^{III} systems that exhibit symmetry-breaking.

Compound	Type of SCO	steps	Cryst. phase	Centers	Spin states	Sym. breaking	Ref
$[Fe^{III}(Him)_2(4MeOhapen)]CF_3SO_3$	abrupt and gradual	2	2	From 1 -> 4	HS -> [3HS-LS]	incomplete	10
$[Fe^{III}(H\text{-}5\text{-}Br\text{-}thsa)(5\text{-}Br\text{-}thsa)]\cdot H_2O$	abrupt and gradual	5/6	4	From 1 -> 4 -> 2 -> 1	[HS] -> [3HS-1LS] -> [HS-LS] -> [LS]	complete	11
$[Fe^{III}(3,5\text{-}OMe\text{-}sal_2bapen)]ClO_4$	gradual	2	3	From 1 -> 3 -> 3	HS -> [2HS-LS] -> [HS-2LS]	incomplete	12
$[Fe^{III}(salpm)_2]ClO_4\cdot 0.5EtOH$	abrupt	2	3	From 2 -> 4 -> 2	[2HS] -> [LS-3HS] -> [2LS]	complete	13
$[Fe^{III}(nsal_2trien)]SCN$	abrupt and gradual	2	3	From 1 -> 2 -> 1	[HS] -> [HS-LS] -> [LS]	complete	14
$[Fe^{III}(qsal\text{-}Br)_2]NO_3\cdot 2MeOH$	abrupt	2	3	From 1 -> 2 -> 1	[HS] -> [HS-LS] -> [LS]	complete	9
$[Fe^{III}(psalpm^{Cl})_2]PTFB$	abrupt	1	2	From 1 -> 2	[HS] -> [HS-LS]	incomplete	15
$[Fe^{III}(qsal\text{-}4\text{-}F)_2]NO_3\cdot 0.91MeOH\cdot 0.57H_2O$	abrupt and gradual	2	2	From 1 -> 2 -> 2	HS -> [HS-LS] -> [LS-LS]	complete	16
$[Fe(qsal)_2][(C_6F_3I_3)I]$	gradual	1	2	From 1 -> 2	[HS] -> [HS-LS]	incomplete	23

Table S4 Crystallographic data and structure refinement of all compounds.

	[Fe(qsal-I)$_2$]NO$_3$·2MeOH									
	1st cooling				**1st warming**			**Dark**	**Irradiated (λ= 660 nm)**	**Irradiated (λ= 980 nm)**
	300 K	**240 K**	**150 K**	**100 K**	**300 K**	**240 K**	**150 K**	**10 K**	**10 K**	**10 K**
Empirical formula	$C_{34}H_{28}FeI_2N_5O_7$									
Formula weight / gmol^{-1}	928.30									
Crystal system	Triclinic									
Space group	$P\bar{1}$	$P\bar{1}$	$P\bar{1}$	$P\bar{1}$	$P\bar{1}$	$P\bar{1}$	$P\bar{1}$	$P\bar{1}$	$P\bar{1}$	$P\bar{1}$
a / Å	12.007(9)	11.965(17)	12.75426(7)	12.732(18)	12.008(3)	11.929(5)	12.754(7)	12.7132(2)	11.9612(5)	11.8742(4)
b / Å	12.471(10)	12.453(18)	13.88144(8)	13.820(16)	12.483(3)	12.458(4)	13.881(8)	13.7693(2)	12.2958(4)	12.3742(3)
c / Å	12.897(5)	12.838(17)	20.01371(9)	20.000(2)	12.908(3)	12.827(5)	20.013(9)	19.9776(3)	12.6524(4)	12.7752(3)
α / °	80.540(5)	80.742(11)	92.0011(4)	91.905(9)	80.487(18)	80.346(3)	92.001(4)	91.9450(10)	82.206(3)	80.502(2)
β / °	69.855(5)	69.681(13)	107.5267(5)	107.56(12)	69.833(19)	69.770(3)	107.526(5)	107.6440(10)	69.547(3)	69.212(3)
γ / °	69.795(7)	69.794(13)	99.7927(5)	99.860(11)	69.770(2)	69.483(3)	99.792(5)	100.0190(10)	69.329(3)	68.990(3)
Cell volume / Å^3	1699.5(2)	1681.8(4)	3315.63(3)	3292.3(7)	1702.1(7)	1672.9(11)	3315.6(3)	3267.76(9)	1631.10(11)	1636.69(9)
Z	2	2	4	4	2	2	4	4	2	2
Absorption coefficient / mm^{-1}	18.295	18.487	18.756	18.889	18.268	18.586	18.756	2.409	2.414	2.405
Reflections collected	25766	24574	95917	44074	22886	24987	95849	52595	19809	23564
Independent reflections, R_{int}	6029, 0.0441	6223, 0.0630	12347, 0.0323	12042, 0.1165	6167, 0.1375	6100, 0.1206	12346, 0.0336	14257, 0.0315	6903, 0.0500	7147, 0.0436
Max. and min. transmission	0.427 0.032	0.656 0.178	0.867 0.315	0.301 0.031	0.352 0.056	0.295 0.020	0.521 0.156	0.764 0.590	0.945 0.747	0.962 0.766
Restrains/parameters	0/446	0/446	0/891	144/891	0/441	1/446	0/891	89/931	0/446	0/446
Final R indices [I>=2σ (I)]	0.0544	0.0428	0.0375	0.0675	0.0601	0.0712	0.0373	0.0295	0.0401	0.0315
R_1, wR_2	0.1592	0.1171	0.1035	0.1757	0.1673	0.2064	0.1035	0.0701	0.0772	0.0623
CCDC No.	2220036	2220037	2220038	2220039	2220040	2220041	2220042	2220043	2220044	2220045

	$[Fe(qsal\text{-}I)_2]NO_3 \cdot 2EtOH$	
	300 K	**150 K**
Empirical formula	$C_{36}H_{32}FeI_2N_5O_7$	
Formula weight / gmol^{-1}	956.30	
Crystal system	Triclinic	
Space group	$P\bar{1}$	$P\bar{1}$
a / Å	12.295(3)	12.079(13)
b / Å	12.335(3)	12.309(12)
c / Å	13.121(3)	12.907(11)
α / °	81.189(19)	72.615(8)
β / °	71.562(2)	82.731(8)
γ / °	71.229(2)	71.135(9)
Cell volume / Å^3	1784.5(8)	1732.3(3)
Z	2	2
Absorption coefficient / mm^{-1}	17.447	17.973
Reflections collected	26380	27592
Independent reflections, R_{int}	6412, 0.0601	6318, 0.0429
Max. and min. transmission	0.485, 0.216	0.504, 0.229
Restrains/parameters	15/549	0/539
Final R indices [I>=2σ (I)]	0.0402	0.0293
R_1, wR_2	0.0988	0.0718
CCDC No.	2220046	2220047

Table S5 Distances between the chains (d_{chain}) and the planes (d_{plane}) at different temperatures (LT = low temperature, RT = room temperature, HT = high temperature).

		$[Fe(qsal\text{-}I)_2]NO_3 \cdot 2MeOH$				$[Fe(qsal\text{-}I)_2]NO_3 \cdot 2EtOH$		$[Fe(qsal\text{-}Br)_2]NO_3 \cdot 2MeOH$	
		d_{plane}		d_{chain}		d_{plane}	d_{chain}	d_{plane}	d_{chain}
1st cooling	**300 K**	12.472		12.008		12.335	12.295	12.325	12.02
	240 K	12.459		11.929		-	-	-	-
	150 K	12.475	12.262	12.231	11.724	12.080	12.309	12.304 12.073	12.273 11.779
	100 K	-		-		-	-	12.119	12.080
1st warming	**300 K**	12.472		12.008		-	-	-	-
2nd cooling	**240 K**	12.454		11.965		-	-	-	-
	150 K	12.469	12.267	12.247	11.717	-	-	-	-
Dark	**10 K**	12.412	12.237	12.191	11.684			-	-
Irradiated (λ= 660 nm)	**10 K**	12.296		11.961		-	-	-	-
Irradiated (λ= 980 nm)	**10 K**	12.374		11.874				-	-

Table S6 List of Fe^{III} systems that exhibit photoactivation.[17]

Iron(III) Complex	Meta-Stable HS state	T(LIESST)	Thermal SCO behavior	Ref
$[Fe(qsal\text{-}I)_2]NO_3 \cdot 2MeOH$	67 % at 10 K	38 K	Abrupt, no hysteresis ($T_{1/2}$ = 210 K)	This work
	35 % at 10 K reverse-LIESST	45 K	Gradual, no hysteresis	
$[Fe(qsal)_2]NCS \cdot CH_2Cl_2$	17 % at 5 K	20 K	Abrupt, hysteresis ($T_{1/2}$ (↑) = 210, 290 K, $T_{1/2}$ (↓) = 203 K)	18
$[Fe(qsal)_2]NCSe \cdot CH_2Cl_2$	8% at 5 K	50 K	Abrupt, hysteresis ($T_{1/2}$ (↑) = 282 K, $T_{1/2}$ (↓) = 212 K)	18
$[Fe(qsal)_2]C_6H_5SO_3 \cdot MeOH$	59 % at 5 K	50 K	Abrupt, hysteresis ($T_{1/2}$ (↑) = 205 K, $T_{1/2}$ (↓) = 195 K)	19
$[Fe(qsal)_2][Ni(dmit)_2] \cdot 2MeCN$	14 % at 5 K	46 K	Abrupt, no hysteresis ($T_{1/2}$ = 231 K)	20
$[Fe(I\text{-}qsal)_2][Ni(dmit)_2] \cdot MeCN \cdot H_2O$	43 % at 5 K	75 K[a]	Abrupt, hysteresis ($T_{1/2}$ (↑) = 156 K, $T_{1/2}$ (↓) = 150 K)	21
$[Fe(azp)(qsal)] \cdot 0.5MeOH$	21 % at 5 K	55 K[a]	Abrupt, hysteresis ($T_{1/2}$ (↑) = 192 K, $T_{1/2}$ (↓) = 182 K)	22
$[Fe(qsal)_2][(C_6F_3I_3)I]$	59 % at 10 K	45 K	Gradual, no hysteresis	23
$[Fe(qsal)_2]_2[Fe(CN)_5NO] \cdot MeOH$	60 % at 5 K	45 K	Gradual, no hysteresis ($T_{1/2}$ = 122 K)	24
$[Fe(qsal)_2]_2[Ru(Cl)_5(NO)] \cdot 2.5H_2O$	20 % at 10 K	45 K[a]	Gradual, hysteresis ($T_{1/2}$ (↑) = 190 K, $T_{1/2}$ (↓) = 183 K)	25
$[Fe(naphBzen)_2]I$	15 % at 10 K	40-70 K[a]	Abrupt, hysteresis [HS-HS]<->[HS-LS] ($T_{1/2}$ (↑) = 135 K, $T_{1/2}$ (↓) = 110 K	26
	50 % at 10 K reverse-LIESST	60 K[b]	Abrupt, hysteresis [LS-LS]<->[HS-LS] ($T_{1/2}$ (↑) = 60 K, $T_{1/2}$ (↓) = 30 K	
$[Fe(pap)_2]ClO_4 \cdot H_2O$	59% at 5 K	105 K	Abrupt, hysteresis ($T_{1/2}$ (↑) = 181 K, $T_{1/2}$ (↓) = 165 K)	27
$[Fe(pap)_2]BF_4 \cdot H_2O$	50 % at 5 K	100 K	Abrupt, hysteresis ($T_{1/2}$ (↑) = 195 K, $T_{1/2}$ (↓) = 170 K)	18
$[Fe(pap)_2]PF_6 \cdot MeOH$	25 % at 5 K	55 K	Abrupt, hysteresis ($T_{1/2}$ (↑) = 293 K, $T_{1/2}$ (↓) = 291 K)	28

$[Fe(qnal)_2]OTf \cdot MeOH$	52 % at 5 K	75 K	Abrupt, hysteresis ($T_{1/2}$ (↑) = 115 K, $T_{1/2}$ (↓) = 104 K)	29
$[Fe(qnal)_2]OTf \cdot acetone$	100 % at 5 K	58 K	Abrupt, hysteresis ($T_{1/2}$ (↑) = 133 K, $T_{1/2}$ (↓) = 130 K)	29
$[Fe(qnal)_2][Pd(dmit)_2]_5 \cdot acetone$	10 % at 5 K[a]	30 K[a]	Gradual, no hysteresis	30
$[Fe(qnal)_2]C_{10}H_7SO_3$	23 % at 5 K	45 K	Abrupt, hysteresis ($T_{1/2}$ (↑) = 219 K, $T_{1/2}$ (↓) = 188 K)	19
$[Fe(qnal)_2]C_{16}H_9SO_3 \cdot MeOH \cdot CH_2Cl_2$	44 % at 5 K	62 K	Abrupt, no hysteresis ($T_{1/2}$ = 240 K)	19
$[Fe(qnal)_2]BPh_4 \cdot CH_2Cl_2$	65 % at 5 K	25 K	Gradual, no hysteresis ($T_{1/2}$ = 285 K)	31
$[Fe(qnal\text{-}OMe)_2]PF_6 \cdot acetone$	90 % at 5 K	60 K	Abrupt, hysteresis ($T_{1/2}$ (↑) = 202 K, $T_{1/2}$ (↓) = 194 K)	32
$[Fe(qnal\text{-}OMe)_2]BPh_4 \cdot 2MeOH$	87 % at 5 K	100 K	Abrupt, hysteresis ($T_{1/2}$ (↑) = 304 K, $T_{1/2}$ (↓) = 194 K)	32
$[Fe(Hphsalpm^{Cl})_2]PTFB \cdot MeOH$	96 % at 10 K	53 K	Gradual, no hysteresis ($T_{1/2}$ = 153 K)	15
$[Fe(Hphsalpm^{Br})_2]PTFB \cdot MeOH$	96 % at 10 K	42 K	Gradual, no hysteresis ($T_{1/2}$ = 220 K)	15
$[Fe(Hphsalpm^{I})_2]PTFB \cdot MeOH$	28 % at 10 K (reverse-LIESST)	37 K	No transition, high spin only	15
$[Fe(salpm)_2]ClO_4 \cdot 0.5EtOH$	80 % at 10 K[a]	40, 50 K	Abrupt, no hysteresis ($T_{1/2}$ = 115, 171 K)	33
[Fe(thpu)(Hthpu)]	~2 % at 20 K[a]	40 K	Abrupt, hysteresis ($T_{1/2}$ (↑) = 239 K, $T_{1/2}$ (↓) = 225 K)	34
(TMA)$[Fe(azp)_2]$	59 % at 5 K[a]	68 K[a]	Gradual, no hysteresis	35
$[Fe(H\text{-}5\text{-}Cl\text{-}thsa\text{-}Me)(5\text{-}Cl\text{-}thsa\text{-}Me)] \cdot H_2O$	16 % at 10 K	40 K	Abrupt, hysteresis ($T_{1/2}$ (↑) = 249, 278 K, $T_{1/2}$ (↓) = 245, 270 K)	36

[a]The percentage and temperature were estimated from the apparent values in the original papers.

[b]The transition temperature is for LS to an intermediate-HS state, based on the reverse-LIESST process.

Table S7 Intermolecular interactions of all compounds (Å).

			$[Fe(qsal\text{-}I)_2]NO_3 \cdot 2MeOH$											
					1st cooling		1st warming		2nd cooling		Dark		Irradiated (660 nm)	Irradiated (980 nm)
			300 K	240 K	150 K		300 K	240 K	150 K		10 K		10 K	10 K
1D chains														
Fe-Fe					Fe1-Fe1	Fe2-Fe2			Fe1-Fe1	Fe2-Fe2	Fe1-Fe1	Fe2-Fe2		
	π-π (Type A)	Cent-plane	3.470	3.454	3.379	3.443	3.452	3.438	3.374	3.437	3.262	3.418	3.367	3.421
	π-π (Type B)	Cent-plane	3.340	3.327	3.285	3.322	3.340	3.328	3.327	3.319	3.362	3.297	3.268	3.287
	C-H···O	O1-H23	2.608	2.721	2.732	2.760	2.594	2.594	2.730	2.763	2.615	2.643	2.625	2.540
	C-H···O	O2-H12	2.741	2.803	2.670	2.676	2.689	2.666	2.668	2.678	2.684	2.700	2.647	2.651
	Fe-Fe (Type A)		6.797	6.777	6.938	6.688	6.746	6,767	6.935	6.686	6.917	6.660	6.835	6.707
	Fe-Fe (Type B)		7.265	7.223	7.272	7.156	7.226	7.209	7.276	7.151	7.241	7.120	7.179	7.161
MeOH	OH_m···C-H	O7-H10	2.487	2.504	2.572	2.473	2.466	2.487	2.571	2.473	2.541	2.457	2.525	2.453
	OH_m···OH_m	O7-H31	1.989	1.910	1.913	1.898	1.891	1.878	1.910	1.898	1.882	1.882	1.889	1.883
NO_3	O···C-H	O3-H15	2.690	2.674	2.544	2.642	2.651	2.612	2.543	2.638	2.701	2.367	2.411	2.411
	O···C-H	O3-H1	2.493	2.526	2.382	2.524	2.553	2.462	2.381	2.524	2.684	2.630	2.490	2.612
2D plane														
P4AE	C-H···$C_{centroid}$		2.742	2.725	2.666 / 2.744		2.753	2.713	2.663 / 2.748		2.719 / 2.719		2.680	2.662
	π-π		3.694	3.665	3.606		3.686	3.646	3.603		3.575		3.549	3.608
	C-H···I	I2-H35	3.250	3.244	3.211		3.263	3.247	3.210		3.360		3.224	3.128
MeOH	OH_m···I	O6-I1	3.078	3.064	3.066 / 2.976		3.094	3.077	3.068 / 2.975		-		2.972	3.223
	O···OH_m	O5-H8	2.799	2.039	1.977 / 1.950		2.808	2.801	1.975 / 1.952		1.882		1.889	1.883
NO_3	NO···I	O11-I3	3.502	3.484	3.494 / 3.627		3.508	3.482	3.498 / 3.624		3.486		-	3.448
3D structure														
	C-H···I	I1-H30	3.262	3.242	3.226 / 3.251		3.263	3.244	3.227 / 3.249		3.348		3.229	3.448
	I···I	I2-I2	4.096	4.086	4.084		4.097	4.085	4.084		4.083		4.079	4.034

	[Fe(qsal-I)$_2$]NO$_3$·2EtOH			
			1st cooling	
			300 K	150 K
1D chains				
Fe-Fe				
	π-π (Type A)		3.427	3.325
	π-π (Type B)		3.306	3.264
	C-H···O	O2-H12	2.743	2.577
	C-H···O	O1-H26	2.652	2.840
	C-H···I	I2-H19	3.784	3.769
	Fe-Fe (Type A)		7.014	7.048
	Fe-Fe (Type B)		7.468	7.475
EtOH	OH_e···C-H	O6-H31	-	2.729
	OH_e···C-H	O6-H17	2.241	2.781
	OH_e···N	N2-H33a	2.629	-
NO_3	O···C-H	O3-H1	2.600	2.387
	O···C-H	O3-H15	2.679	2.523
2D plane				
P4AE	CH···$C_{centroid}$		2.902	2.911
	π-π		3.906	3.876
	C-H···I	H3-I2	3.402	3.302
EtOH	OH_e···I		3.185	3.052
	O···OH_e		2.065	1.965
NO_3	NO···I		3.378	3.384
	O···OH_e		2.810	2.782
3D structure				
	C-H···I	I1-H30	3.317	3.235
	I···I	-	-	-

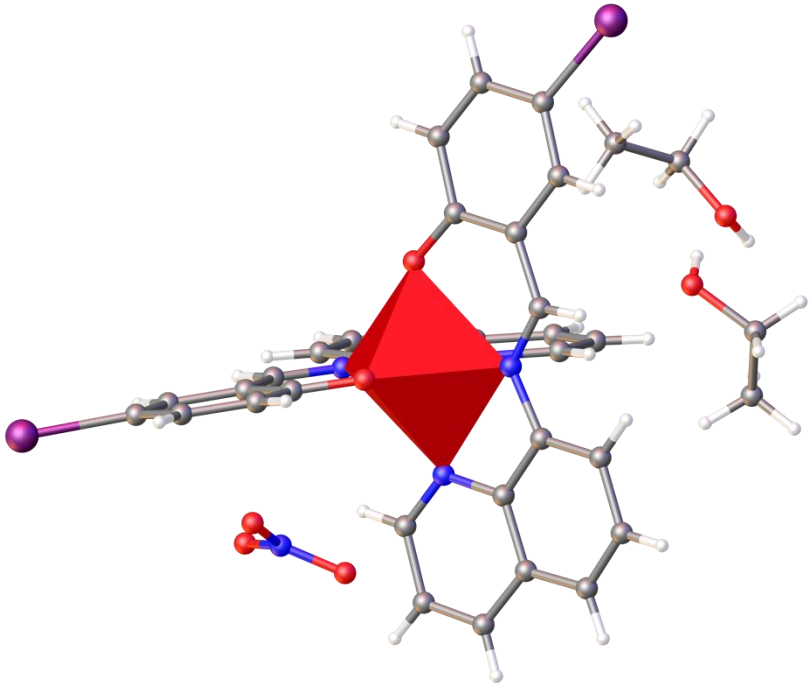

Figure S1 Asymmetric unit of **2** at 150 K.

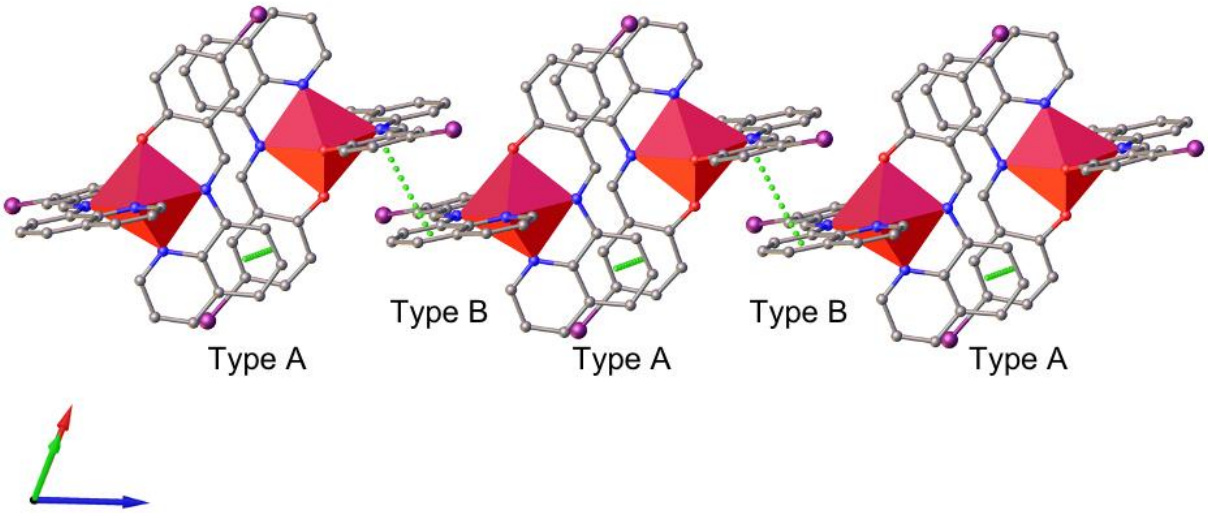

Figure S2 Structure representation of the supramolecular 1D chain for **2** at 150 K.

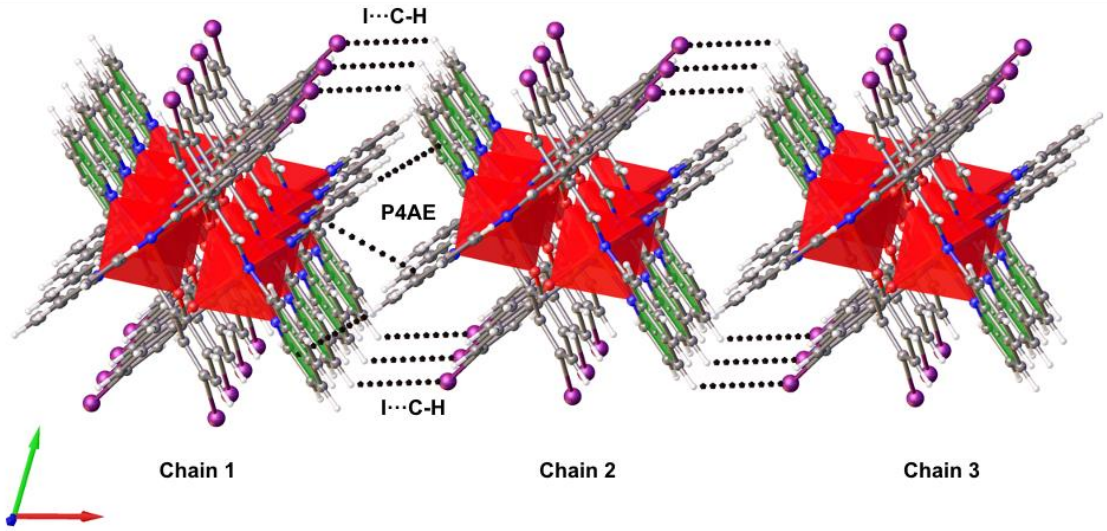

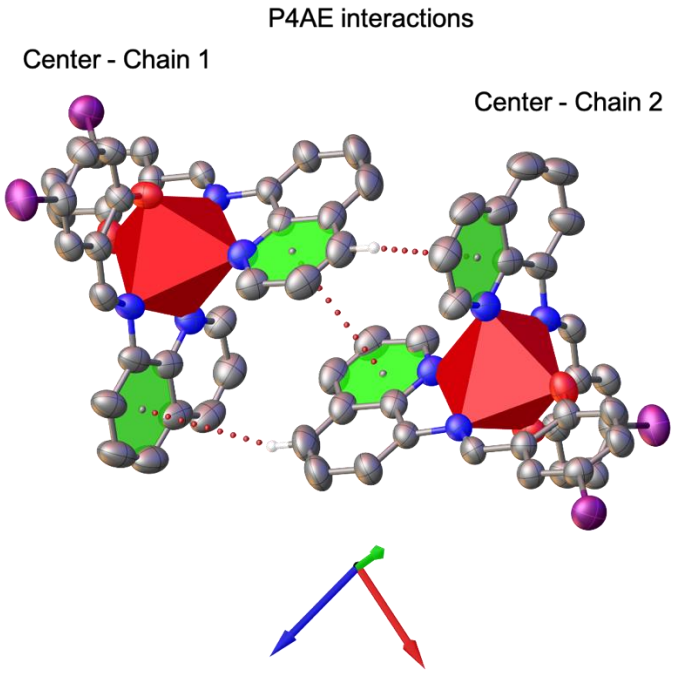

Figure S3 Structure representation of the supramolecular 2D plane **2** at 300 K (top) and view of the P4AE interactions (bottom).

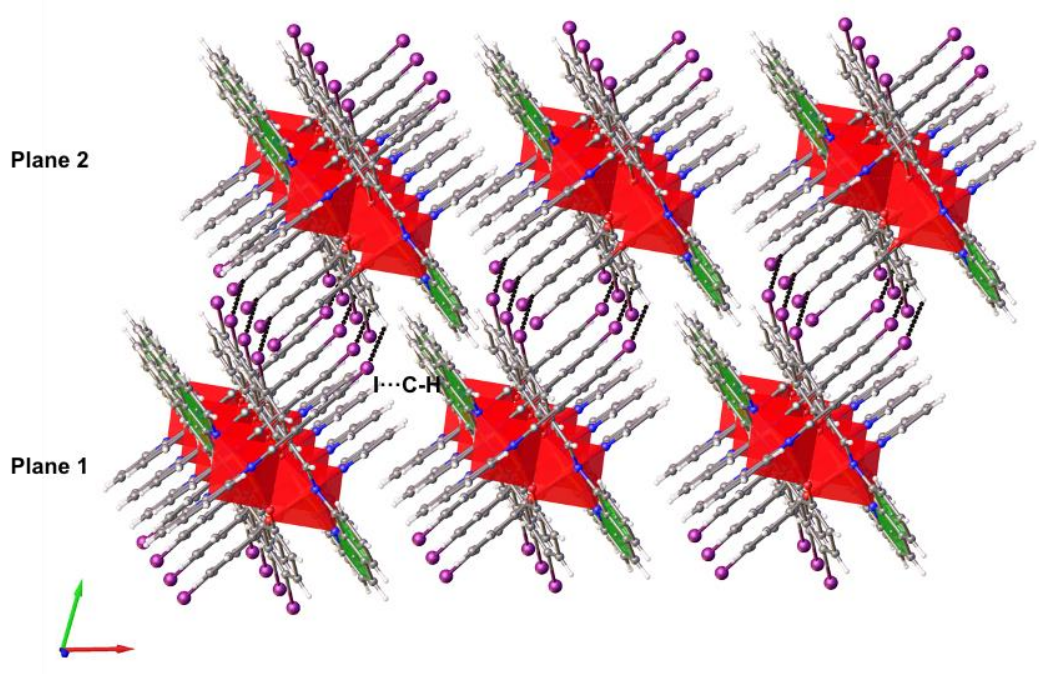

Figure S4 Structure representation of the 3D structure of **2** at 300 K.

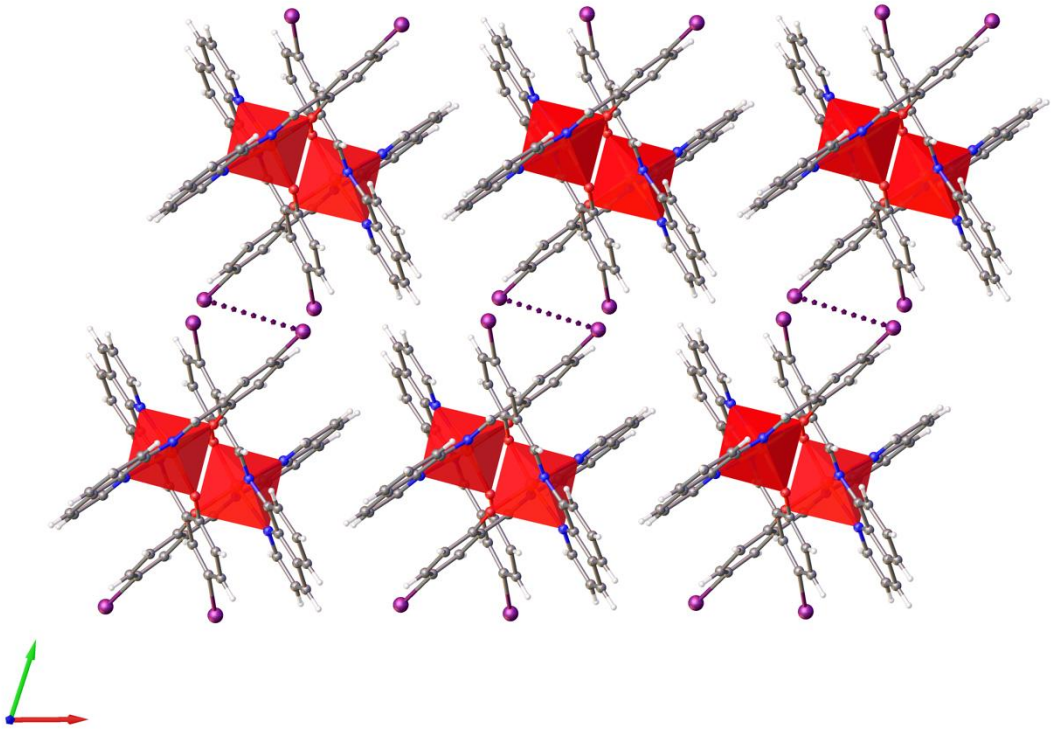

Figure S5 3D structure representation connecting the 2D planes through halogen interactions (I-I) for **1** at 300 K.

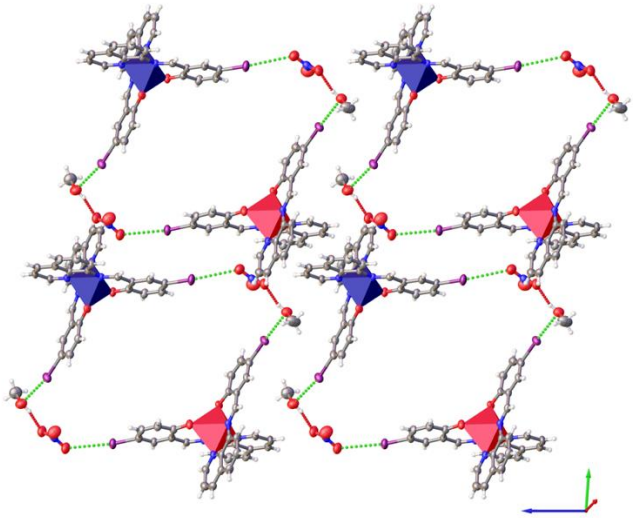

Figure S6: 2D supramolecular square structure connecting different chains involving the methanol and nitrate molecules for **1** at 150 K.

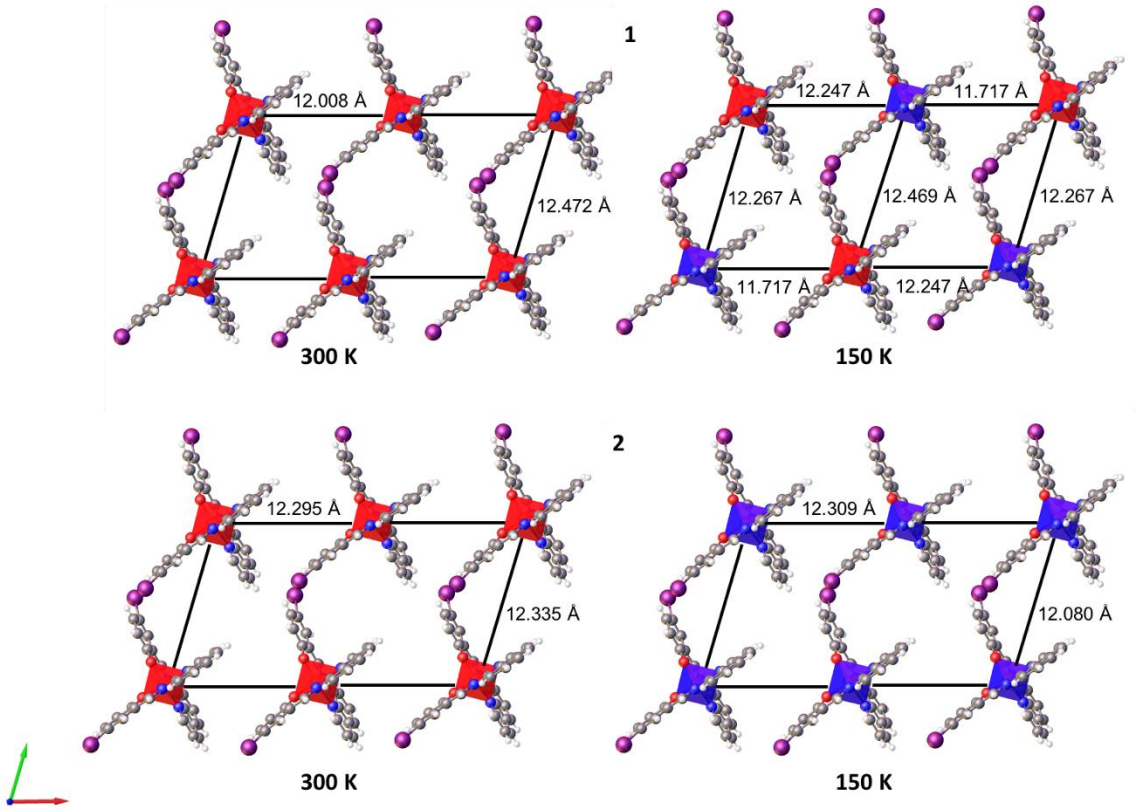

Figure S7 View of d_{chain} (horizontal) and d_{plane} (vertical) of **1** (above) and **2** (below) at 300 K (left) and 150 K (right). Only one Fe per chain is shown for clarity. Red colour represent Fe HS and blue color Fe LS.

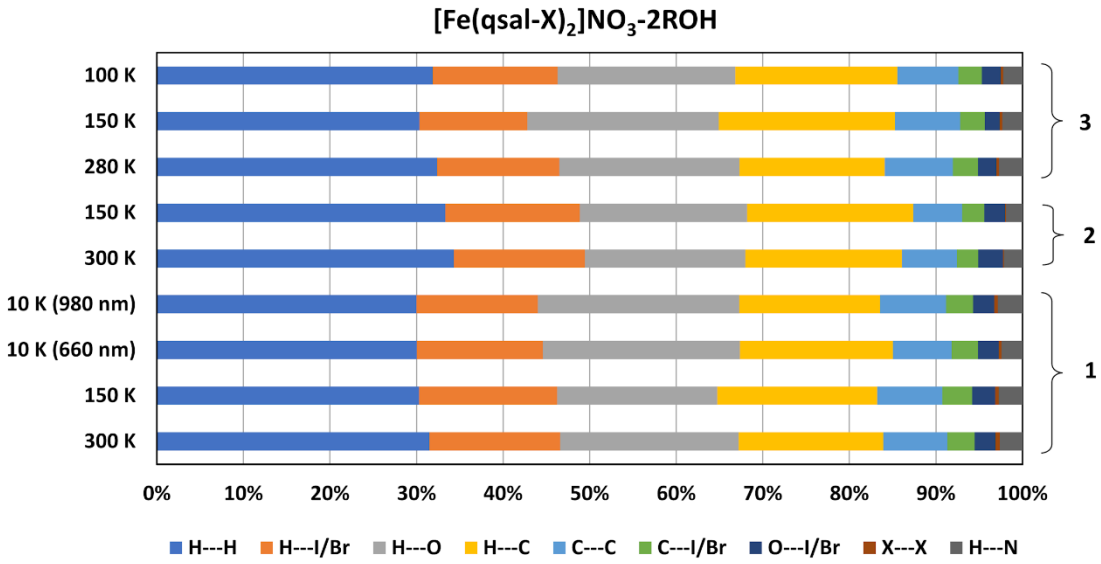

Figure S8 Percentage contributions of interactions for **1**–**3** at all temperatures.

Table S8 Intermolecular interactions contributions for $[Fe(qsal\text{-}I)_2]NO_3{\cdot}2MeOH$ **1**, $[Fe(qsal\text{-}I)_2]NO_3{\cdot}2EtOH$ **2** and $[Fe(qsal\text{-}Br)_2]NO_3{\cdot}2MeOH$.

Ligand	Solvent	Temp	H···H	H···I/Br	H···O	H···C	C···C	C···I/Br	O···I/Br	X···X	H···N
qsal-I	MeOH **1**	300 K	31.3	15.0	20.5	16.6	7.4	3.1	2.4	0.5	2.6
		150 K	29.8	15.7	18.2	18.2	7.4	3.4	2.6	0.4	2.7
		10 K (660 nm)	29.7	14.4	22.5	17.5	6.7	3.0	2.4	0.3	2.4
		10 K (980 nm)	29.5	13.8	22.9	16.0	7.5	3.1	2.4	0.4	2.8
	EtOH **2**	300 K	33.5	14.8	18.1	17.7	6.2	2.4	2.8	0.1	2.1
		150 K	33.3	15.5	19.3	19.2	5.6	2.6	2.4	0.1	1.9
qsal-Br	MeOH	280 K	32.2	14.0	20.7	16.7	7.8	2.9	2.1	0.3	2.7
		150 K	29.9	12.3	21.8	20.1	7.4	2.8	1.7	0.3	2.3
		100 K	31.8	14.4	20.5	18.7	7.0	2.7	2.2	0.3	2.2

all contacts

	$[Fe(qsal\text{-}I)_2]NO_3 \cdot 2MeOH$ **1**	$[Fe(qsal\text{-}I)_2]NO_3 \cdot 2EtOH$ **2**	$[Fe(qsal\text{-}Br)_2]NO_3 \cdot 2MeOH$
300 K	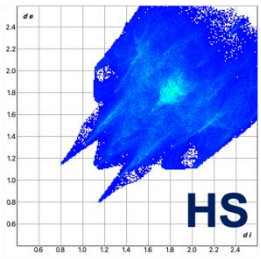	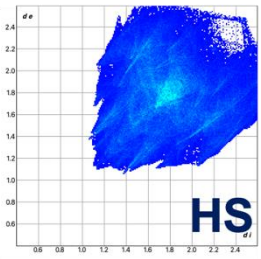	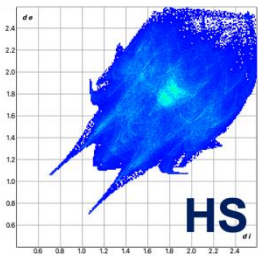
150 K	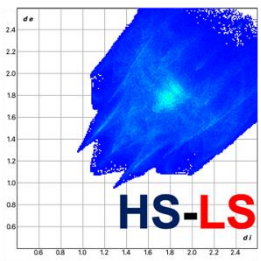	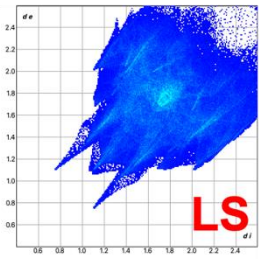	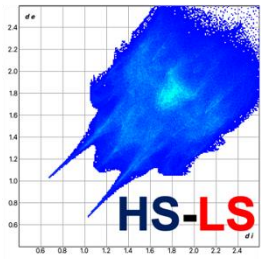
100 K			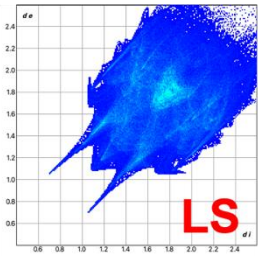
10 K 980 nm (HS)	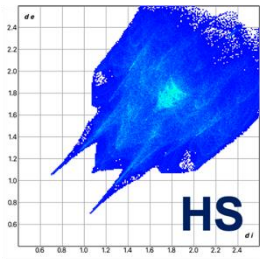		
10 K 660 nm (LS)	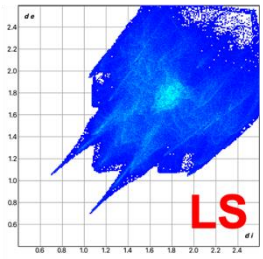		

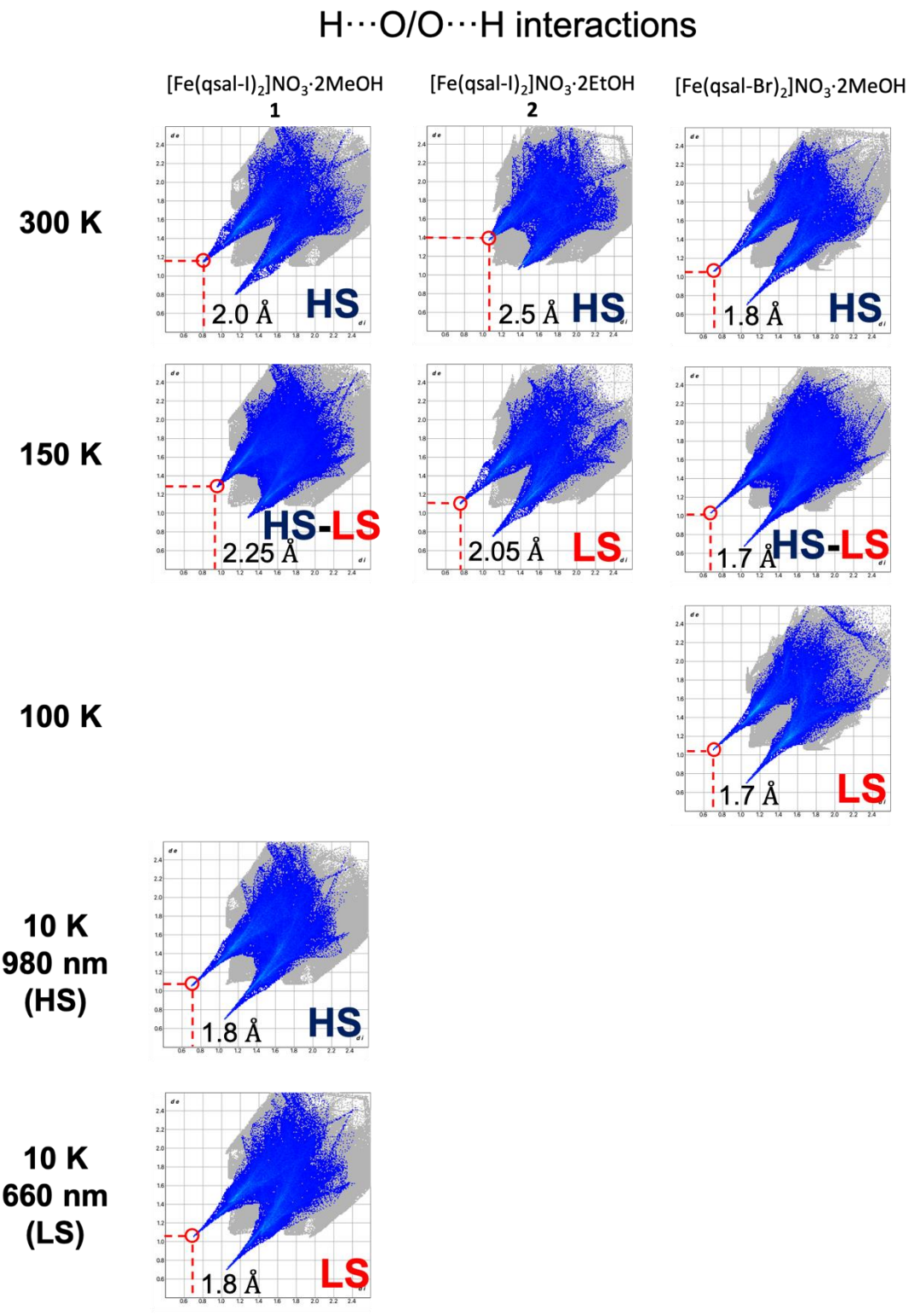

Figure S9 Hirshfeld surface 2D fingerprint plots: all contact (top), H···O/O···H interactions (bottom) for [Fe(qsal-I)$_2$]NO$_3$·2MeOH **1**, [Fe(qsal-I)$_2$]NO$_3$·2EtOH **2** and [Fe(qsal-Br)$_2$]NO$_3$·2MeOH at different temperatures.

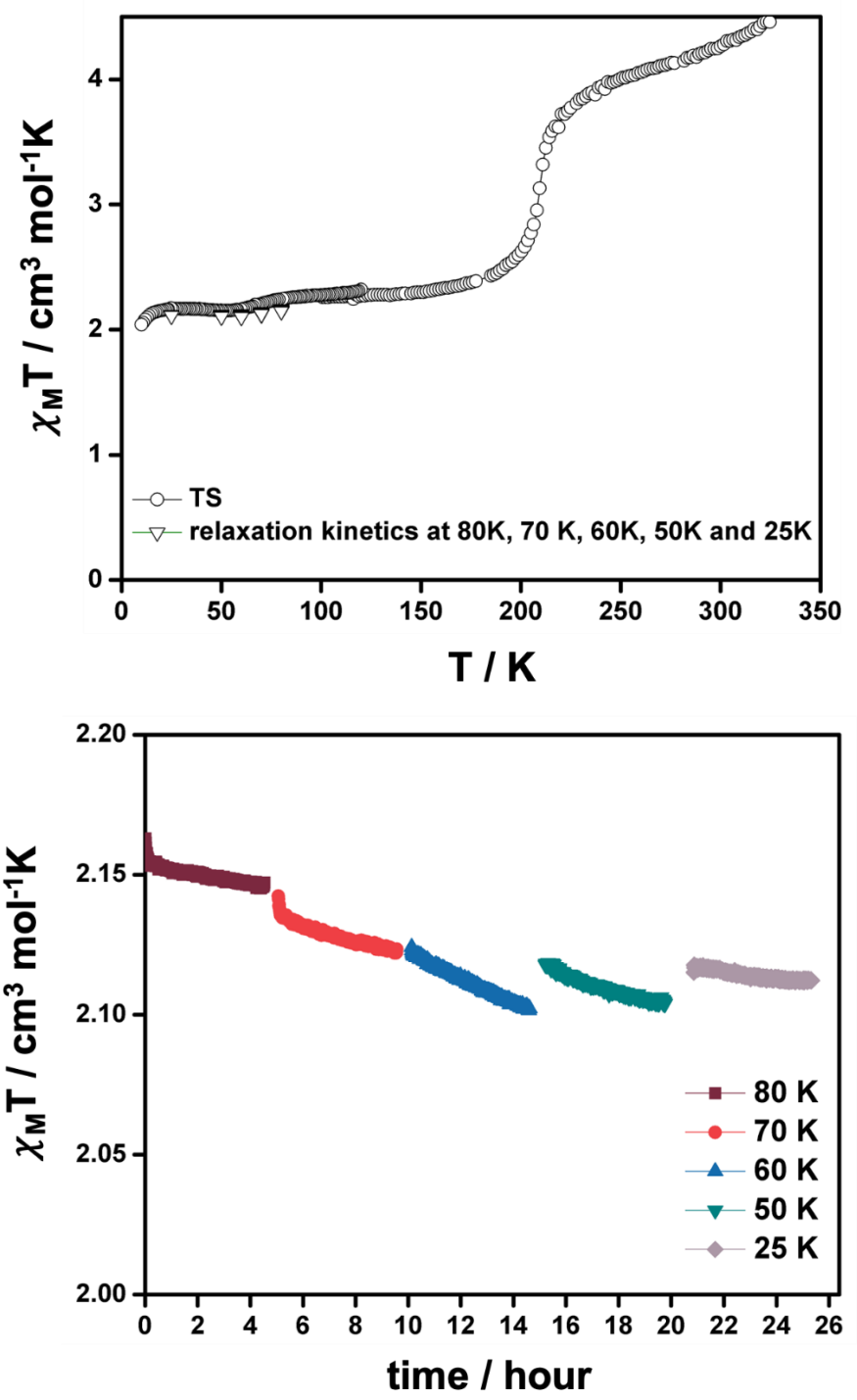

Figure S10 $\chi_M T$ versus T plot of **1** (upper picture). The black diamonds in the upper picture stand for the relaxation kinetics (lower picture) performed from the [HS-LS] state showing the long lifetime of this state.

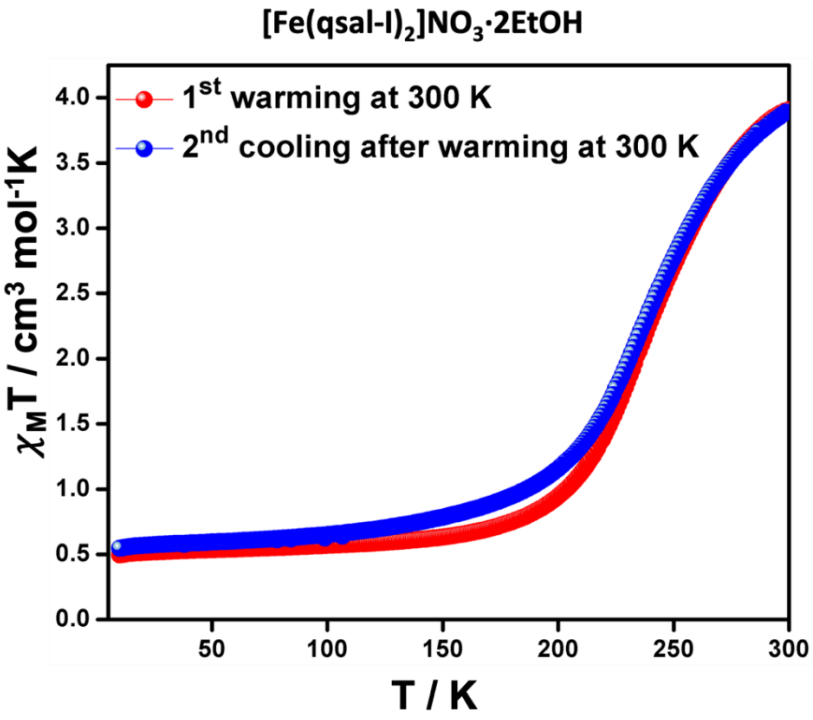

Figure S11 $\chi_M T$ versus T plot of **2** from 10 to 300 K (1st warming) and from 300 to 10 K (2nd cooling).

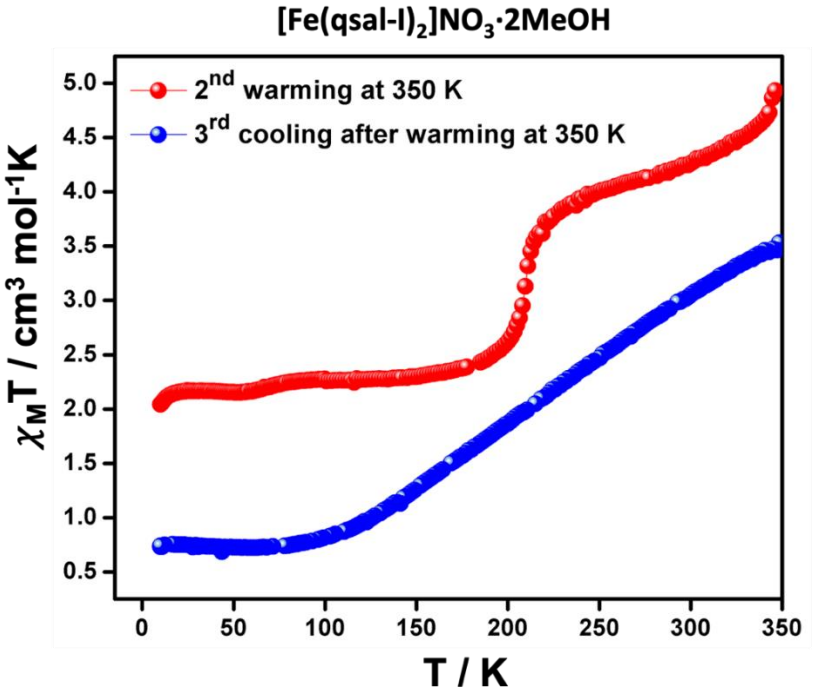

Figure S12 $\chi_M T$ versus T plot of **1** from 10 to 350 K (2nd warming) and from 350 to 10 K (3rd cooling). Data points were measured every K up to 350 K (2nd warming) and then the sample left at 350 K before cooling again. The discontinuity at 350 K may be caused by the combination of some slight decentering caused by the increasing temperature and the loss of solvent (MeOH).

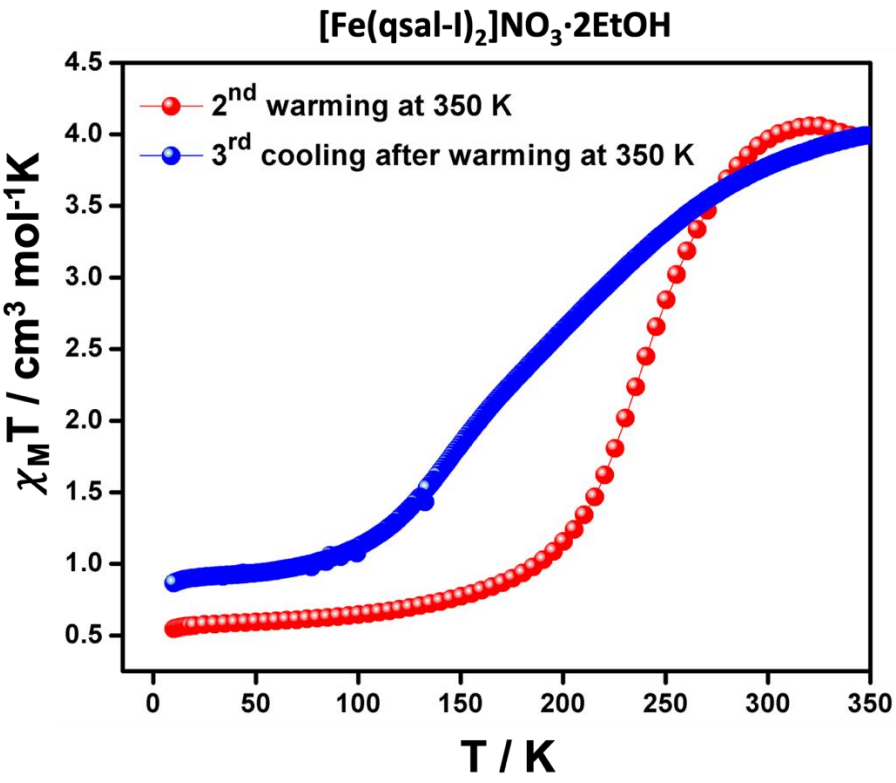

Figure S13 $\chi_M T$ versus T plot of **2** from 10 to 350 K (2nd warming) and from 350 to 10 K (3rd cooling).

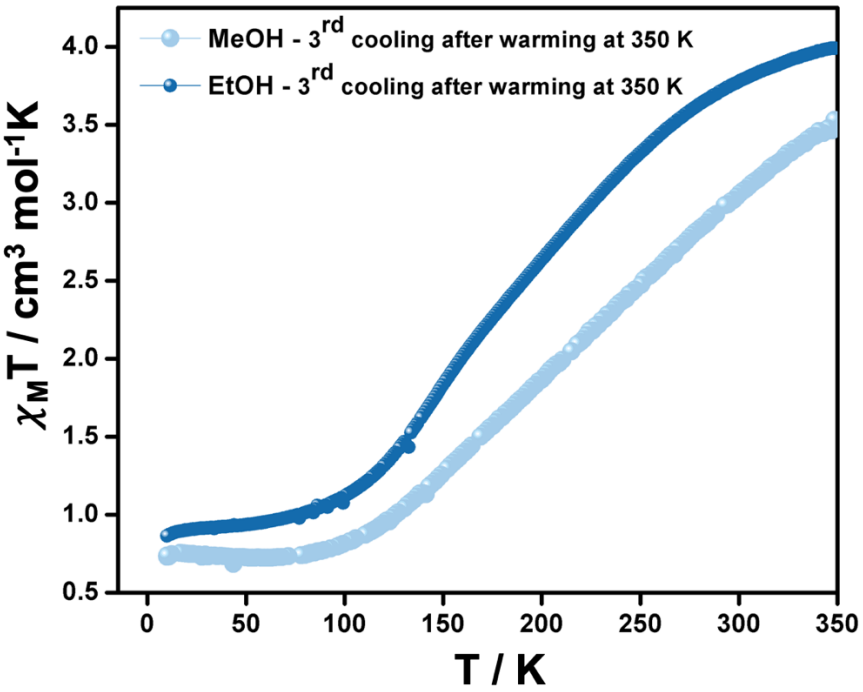

Figure S14 $\chi_M T$ versus T plot of **1** (light blue) and **2** (dark blue) from 350 to 10 K (3rd cooling).

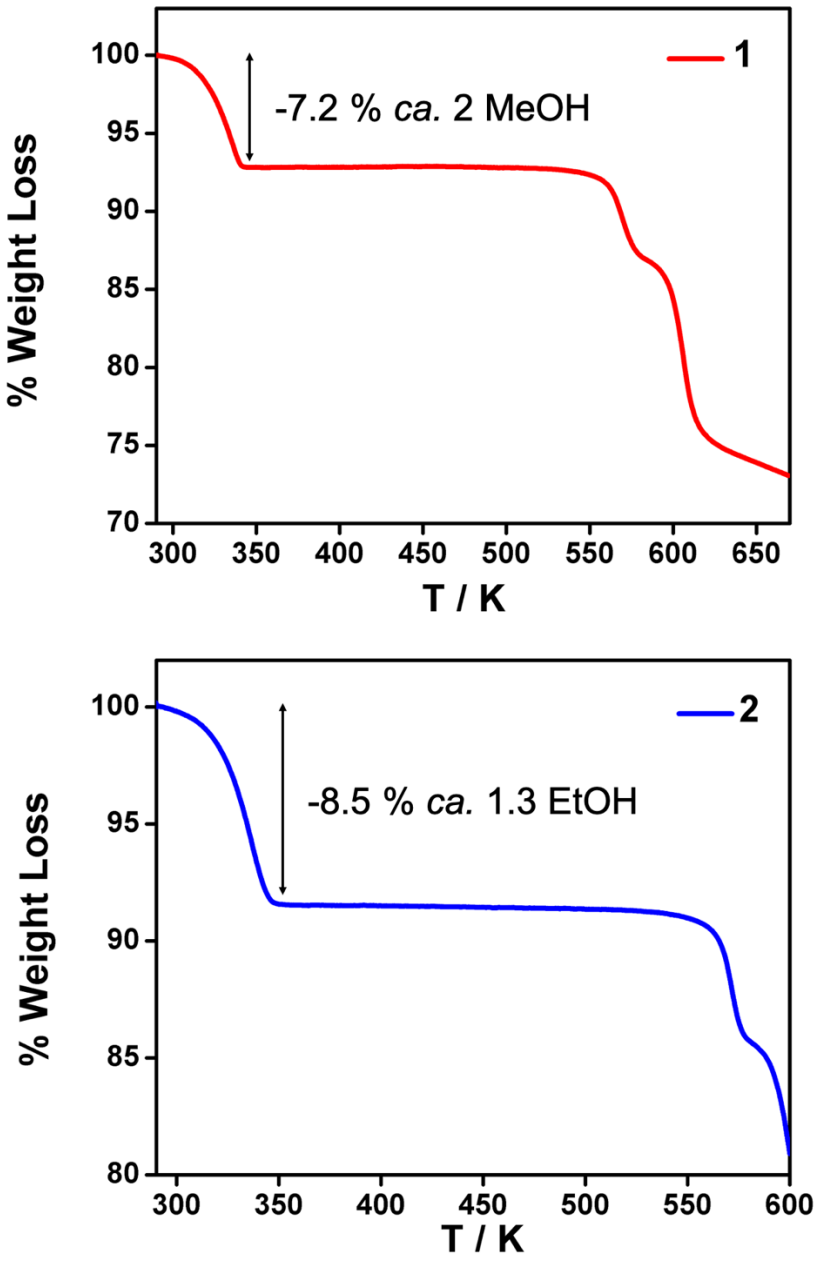

Figure S15 TGA curves for 1 (red) and 2 (blue).

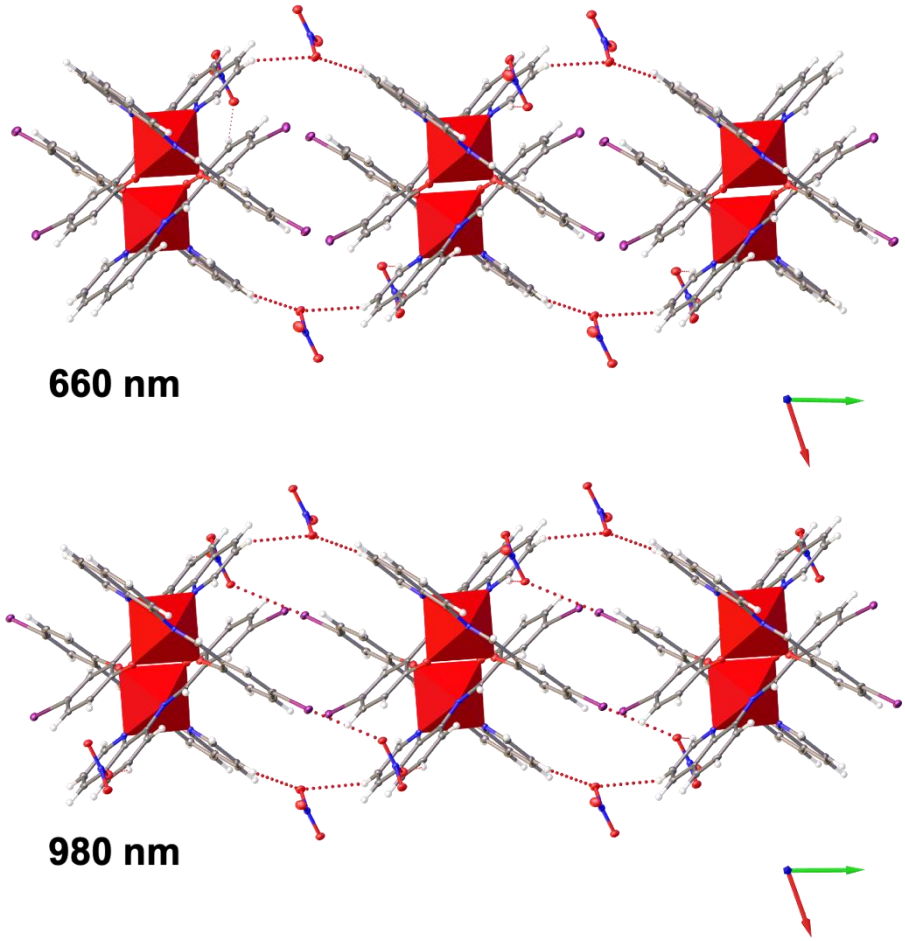

Figure S16 Structure representation of the 2D supramolecular structure showing the I···O(nitrate) halogen bond in **1** upon irradiation at 660 nm (top) and 980 nm (bottom).

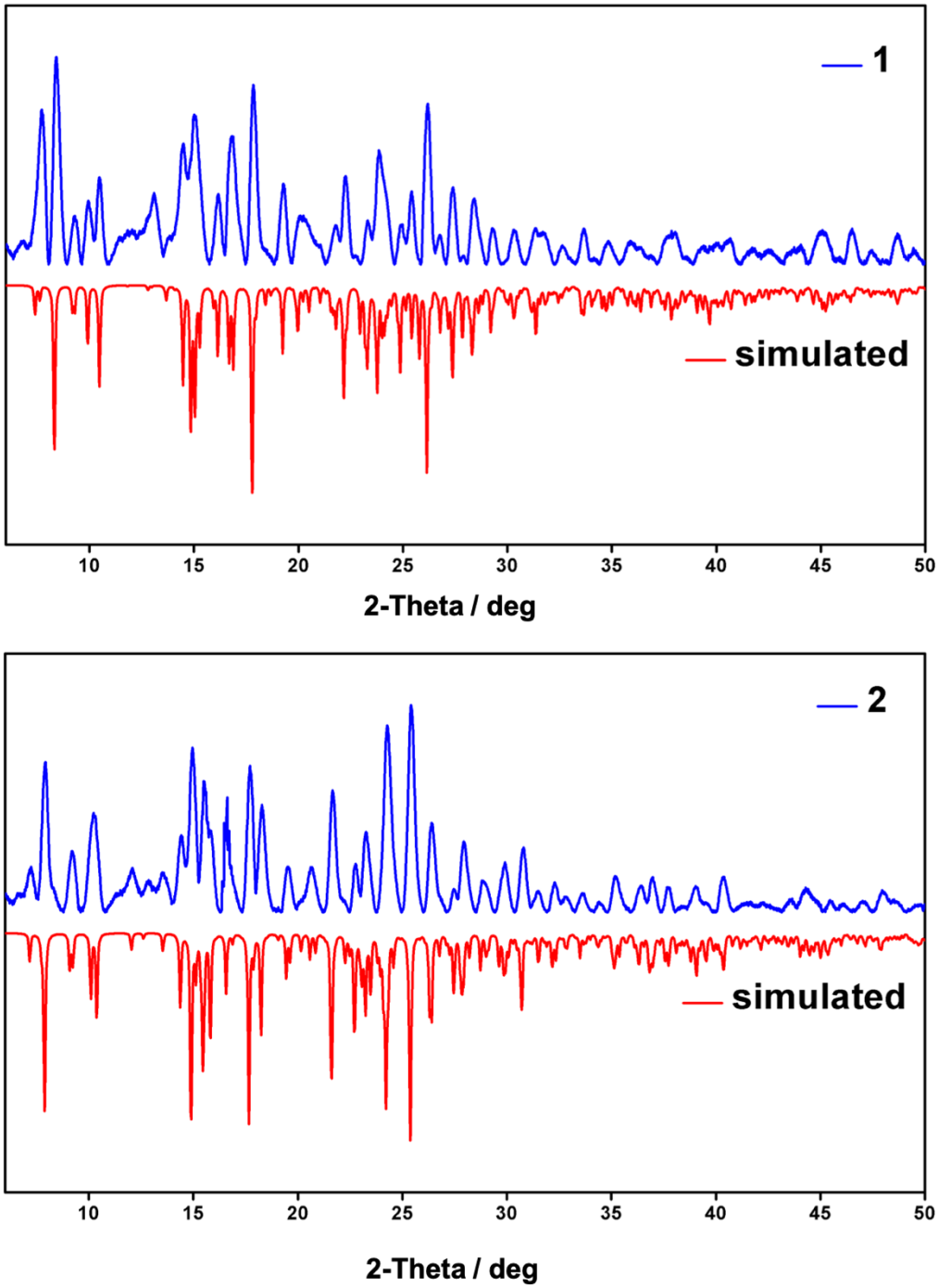

Figure S17 Experimental PXRD diffractograms (blue) and the corresponding simulated patterns (red) for **1** (up) and **2** (down) at room temperature.

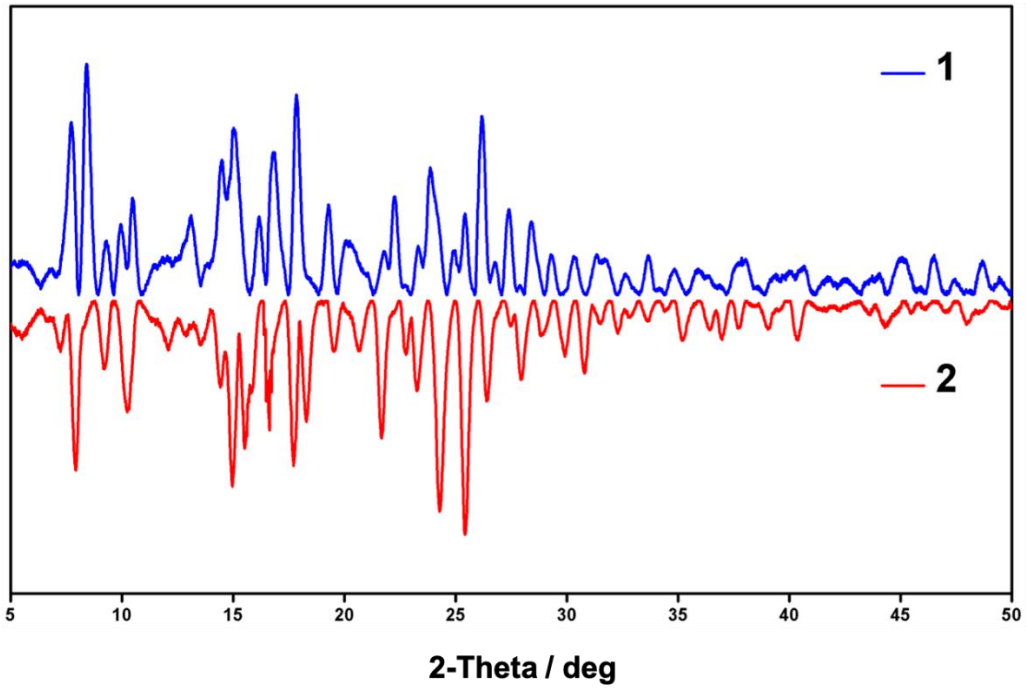

Figure S18 Comparison of the experimental PXRD diffractograms of **1** (blue) and **2** (red) at room temperature.

References

1 J. Sirirak, W. Phonsri, D. J. Harding, P. Harding, P. Phommon, W. Chaoprasa, R. M. Hendry, T. M. Roseveare and H. Adams, *J. Mol. Struct.*, 2013, **1036**, 439–446.

2 1996.

3 G. M. Sheldrick, *Acta Crystallogr. Sect. A Found. Adv.*, 2015, **71**, 3–8.

4 G. M. Sheldrick, *Acta Crystallogr. Sect. C Struct. Chem.*, 2015, **71**, 3–8.

5 O. V. Dolomanov, L. J. Bourhis, R. J. Gildea, J. A. K. Howard and H. Puschmann, *J. Appl. Crystallogr.*, 2009, **42**, 339–341.

6 G. Chastanet, C. Desplanches, C. Baldé, P. Rosa, M. Marchivie and P. Guionneau, *Chem. Squared*, 2018, **2**, 2.

7 J. F. Létard, L. Capes, G. Chastanet, N. Moliner, S. Létard, J. A. Real and O. Kahn, *Chem. Phys. Lett.*, 1999, **313**, 115–120.

8 G. Chastanet, C. Desplanches, M. Gonidec, P. Guionneau, M. Marchivie, C. Mathonière and P. Rosa, *Light-Induced Excited Spin-State Trapping: A Methodological Approach*, Elsevier Inc., 2021.

9 D. J. Harding, W. Phonsri, P. Harding, K. S. Murray, B. Moubaraki and G. N. L. Jameson, *Dalton Trans.*, 2015, **44**, 15079–15082.

10 K. Miyano, T. Nishida, H. Ono, D. Hamada, T. Fujinami, N. Matsumoto and Y. Sunatsuki, *Inorg. Chim. Acta*, 2016, **439**, 49–54.

11 Z.-Y. Li, H. Ohtsu, T. Kojima, J.-W. Dai, T. Yoshida, B. K. Breedlove, W.-X. Zhang, H. Iguchi, O. Sato, M. Kawano and M. Yamashita, *Angew. Chem. Int. Ed.*, 2016, **55**, 5184–5189.

12 M. Griffin, S. Shakespeare, H. J. Shepherd, C. J. Harding, J.-F. Létard, C. Desplanches, A. E. Goeta, J. A. K. Howard, A. K. Powell, V. Mereacre, Y. Garcia, A. D. Naik, H. Müller-Bunz and G. G. Morgan, *Angew. Chem. Int. Ed.*, 2011, **50**, 896–900.

13 K. D. Murnaghan, C. Carbonera, L. Toupet, M. Griffin, M. M. Dîrtu, C. Desplanches, Y. Garcia, E. Collet, J. F. Létard and G. G. Morgan, *Chem. - A Eur. J.*, 2014, **20**, 5613–5618.

14 B. J. C. Vieira, J. T. Coutinho, I. C. Santos, L. C. J. Pereira, J. C. Waerenborgh and V. Da Gama, *Inorg. Chem.*, 2013, **52**, 3845–3850.

15 Z. Liu, Z. Yao and J. Tao, *Inorg. Chem.*, 2021, **60**, 10291–10301.

16 H. J. Sheng, C. C. Xia, X. Y. Zhang, C. C. Zhang, W. J. Ji, Y. Zhao and X. Y. Wang, *Inorg. Chem.*, 2022, **61**, 12726–12735.

17 M. Nakaya, R. Ohtani, L. F. Lindoy and S. Hayami, *Inorg. Chem. Front.*, 2021, **8**, 484–498.

18 S. Hayami, K. Hiki, T. Kawahara, Y. Maeda, D. Urakami, K. Inoue, M. Ohama, S. Kawata and O. Sato, *Chem. - A Eur. J.*, 2009, **15**, 3497–3508.

19 A. Tsukiashi, M. Nakaya, F. Kobayashi, R. Ohtani, M. Nakamura, J. M. Harrowfield, Y. Kim and S. Hayami, *Inorg. Chem.*, 2018, **57**, 2834–2842.

20 K. Takahashi, H. Cui, H. Kobayashi, Y. Einaga and O. Sato, *Chem. Lett.*, 2005, **34**, 1240–1241.

21 K. Fukuroi, K. Takahashi, T. Mochida, T. Sakurai, H. Ohta, T. Yamamoto, Y. Einaga and H. Mori, *Angew. Chem. Int. Ed.*, 2014, **53**, 1983–1986.

22 S. Murata, K. Takahashi, T. Mochida, T. Sakurai, H. Ohta, T. Yamamoto and Y. Einaga, *Dalton Trans.*, 2017, **46**, 5786–5789.

23 I.-R. Jeon, C. Mathonière, R. Clérac, M. Rouzières, O. Jeannin, E. Trzop, E. Collet and M. Fourmigué, *Chem. Commun.*, 2017, **53**, 10283–10286.

24 T. Togo, S. A. Amolegbe, R. Yamaguchi, T. Kuroda-Sowa, M. Nakaya, K. Shimayama, M. Nakamura and S. Hayami, *Chem. Lett.*, 2013, **42**, 1542–1544.

25 C. Faulmann, J. Chahine, L. Valade, G. Chastanet, J. Létard and D. de Caro, *Eur. J. Inorg. Chem.*, 2013, **2013**, 1058–1067.

26 T. Boonprab, S. J. Lee, S. G. Telfer, K. S. Murray, W. Phonsri, G. Chastanet, E. Collet, E.

Trzop, G. N. L. Jameson, P. Harding and D. J. Harding, *Angew. Chem. Int. Ed.*, 2019, **58**, 11811–11815.
27 S. Hayami, Z. Gu, M. Shiro, Y. Einaga, A. Fujishima and O. Sato, *J. Am. Chem. Soc.*, 2000, **122**, 7126–7127.
28 G. Juhász, S. Hayami, O. Sato and Y. Maeda, *Chem. Phys. Lett.*, 2002, **364**, 164–170.
29 T. Shimizu, Y. Komatsu, H. Kamihata, Y. H. Lee, A. Fuyuhiro, S. Iijima and S. Hayami, *J. Incl. Phenom. Macrocycl. Chem.*, 2011, **71**, 363–369.
30 K. Takahashi, H.-B. Cui, Y. Okano, H. Kobayashi, H. Mori, H. Tajima, Y. Einaga and O. Sato, *J. Am. Chem. Soc.*, 2008, **130**, 6688–6689.
31 W. Thammasangwan, P. Harding, S. G. Telfer, A. Alkaş, W. Phonsri, K. S. Murray, R. Clérac, M. Rouzières, G. Chastanet and D. J. Harding, *Eur. J. Inorg. Chem.*, 2020, **2020**, 1325–1330.
32 M. Nakaya, K. Shimayama, K. Takami, K. Hirata, A. S. Alao, M. Nakamura, L. F. Lindoy and S. Hayami, *Chem. Lett.*, 2014, **43**, 1058–1060.
33 K. D. Murnaghan, C. Carbonera, L. Toupet, M. Griffin, M. M. Dîrtu, C. Desplanches, Y. Garcia, E. Collet, J.-F. Létard and G. G. Morgan, *Chem. - A Eur. J.*, 2014, **20**, 5613–5618.
34 S. Hayami, K. Hashiguchi, K. Inoue and Y. Maeda, *J. Nucl. Radiochem. Sci.*, 2004, **5**, N1–N3.
35 K. Takahashi, K. Kawamukai, M. Okai, T. Mochida, T. Sakurai, H. Ohta, T. Yamamoto, Y. Einaga, Y. Shiota and K. Yoshizawa, *Chem. - A Eur. J.*, 2016, **22**, 1253–1257.
36 Z.-Y. Li, J.-W. Dai, K. J. Gagnon, H.-L. Cai, T. Yamamoto, Y. Einaga, H.-H. Zhao, S. Kanegawa, O. Sato, K. R. Dunbar and R.-G. Xiong, *Dalton Trans.*, 2013, **42**, 14685.